nature physics

ARTICLES
https://doi.org/10.1038/s41567-019-0482-z

Emergence of the geometric phase from quantum measurement back-action

Young-Wook Cho[1,4*], Yosep Kim[2,4], Yeon-Ho Choi[1,3], Yong-Su Kim[1,3], Sang-Wook Han[1], Sang-Yun Lee[1], Sung Moon[1,3] and Yoon-Ho Kim[2*]

The state vector representing a quantum system acquires a phase factor following an adiabatic evolution along a closed trajectory in phase space. This is the traditional example of a geometric phase, or Pancharatnam–Berry phase, a concept that has now been generalized beyond cyclic adiabatic evolutions to include generalized quantum measurements, and that has been experimentally measured in a variety of physical systems. However, a clear description of the relationship between the emergence of a geometric phase and the effects of a series of generalized quantum measurements on a quantum system has not yet been provided. Here we report that a sequence of weak measurements with continuously variable measurement strengths in a quantum optics experiment conclusively reveals that the quantum measurement back-action is the source of the geometric phase—that is, the stronger a quantum measurement, the larger the accumulated geometric phase. We furthermore find that in the limit of strong (projective) measurement there is a direct connection between the geometric phase and the sequential weak value, ordinarily associated with a series of weak quantum measurements.

When a quantum system undergoes adiabatic state evolution along a closed trajectory due to a slow-varying Hamiltonian, it gains a phase factor, now known as the Berry phase[1]. Together with Pancharatnam's phase for polarized light[2,3], the Berry phase is referred to as the geometric phase, because the accumulated phase factor was originally related to the closed geometric path of adiabatic state evolution in an Hilbert space. Over the years, the concept of the geometric phase has been significantly generalized, including non-adiabatic[4], non-cyclic[5,6] and non-unitary state evolutions[7,8], as well as to include evolution of a mixed quantum state[9]. Recently, the geometric phase concept has been found to be applicable in many disciplines, including chemistry[10], materials science[11] and fault-tolerant quantum computing[12,13]. In addition to the theoretical progress, the geometric phase has been observed in a wide variety of physical systems, including photons[14–17], graphene[18], superconducting systems[19], exciton-polariton condensates[20], diamond colour-centres[21], among others.

The generalized geometric phase for non-adiabatic, non-cyclic and non-unitary state evolution can be viewed as the geometric phase induced by a series of generalized quantum measurements. As quantum measurement inevitably involves state disturbance due to quantum measurement back-action[22–24], it has been suggested that quantum measurement back-action is at the heart of the quantum nature of the geometric phase[25]. However, a complete description of the geometric phase for a series of generalized quantum measurements has not yet been reported, either theoretically or experimentally.

In this work, we report an experimental demonstration of the emergence of the geometric phase that results from the quantum measurement back-action generated by a series of generalized quantum measurements. By making use of a sequence of weak quantum measurements with continuously variable measurement strengths, we have conclusively identified the quantum measurement back-action as the origin of the geometric phase—that is, the stronger the measurements, the larger the accumulated geometric phase. Since the measurement interaction in our work is based on a two-qubit entangling operation[26], we clearly demonstrate that the quantum measurement back-action results from the sequential weak quantum measurements. At the strong-measurement limit (that is, projection measurement), this generalized geometric phase is then simplified to the standard geometric phase for well-defined state evolution. We furthermore find that, in the limit of strong projection measurement, there is a direct connection between the geometric phase and the sequential weak value[27–29], ordinarily associated with a series of weak quantum measurements[30–34].

Schematic and theory

We start by considering the geometric aspect of the quantum state change due to sequential quantum measurements. For simplicity, let us first examine the case of sequential quantum measurements for projective observables. The initial quantum state $|\psi\rangle$ is subject to a series of projectors $\hat{A}$, $\hat{B}$ and $\hat{\Pi}^{\phi}=|\phi\rangle\langle\phi|$. The projection postulate states that the sequential observable $\hat{\Pi}^{\phi}\hat{B}\hat{A}$ causes the initial quantum state $|\psi\rangle$ to evolve according to the trajectory $\boldsymbol{\psi}\rightarrow\mathbf{a}\rightarrow\mathbf{b}\rightarrow\boldsymbol{\phi}$ on the Bloch sphere, as shown in Fig. 1a. Note that $\{\boldsymbol{\psi},\mathbf{a},\mathbf{b},\boldsymbol{\phi}\}$ are real vectors in $\mathbb{R}^3$. The closed trajectory is formed by taking $\boldsymbol{\phi}=\boldsymbol{\psi}$. The geometric phase factor $\exp(i\Phi_G)$ emerges from the cyclic quantum state evolution due to the sequential measurement. To measure the geometric phase Φ_G, a phase reference is required and a Mach–Zehnder interferometer provides such a reference (Fig. 1b). The detector exhibits interference according to the dynamical phase difference Δ between the two probability amplitudes. The qubit state in the upper path is subject to the sequential quantum measurement $\hat{\Pi}^{\phi}\hat{B}\hat{A}$, gaining the geometric phase Φ_G, whereas the qubit in the lower path is projected onto the state $|\phi\rangle$ without incurring any geometric phase factor (Fig. 1c). This causes the shift of the interference fringe by the amount Φ_G, which is measurable.

[1]Center for Quantum information, Korea Institute of Science and Technology, Seoul, Korea. [2]Department of Physics, Pohang University of Science and Technology, Pohang, Korea. [3]Division of Nano and Information Technology, KIST School, Korea University of Science and Technology, Seoul, Korea. [4]These authors contributed equally: Young-Wook Cho, Yosep Kim. *e-mail: choyoungwook81@gmail.com; yoonho72@gmail.com

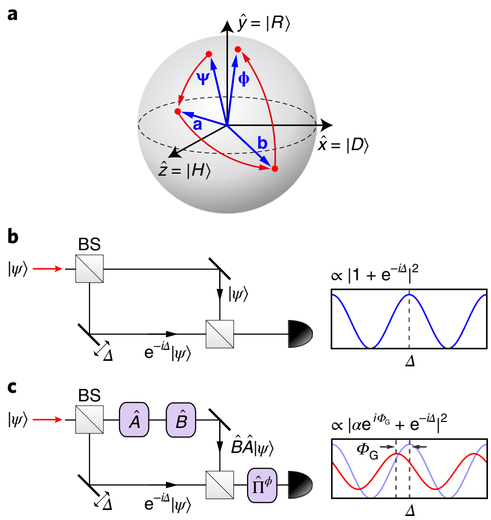

Fig. 1 | Conceptual representation of the geometric phase due to quantum measurement back-action. a. A pure quantum state $|\psi\rangle$ is sequentially measured by projectors $\hat{A}$, $\hat{B}$ and $\hat{\Pi}^{\phi}$, represented by vectors $\{\mathbf{a}, \mathbf{b}, \boldsymbol{\phi}\}$ on the Bloch sphere. The accumulated geometric phase $\exp(i\Phi_G)$ depends on the trajectory $\boldsymbol{\psi} \to \mathbf{a} \to \mathbf{b} \to \boldsymbol{\phi}$. **b**, To measure Φ_G, a phase reference is required and a Mach–Zehnder interferometer provides such a reference: the detector exhibits interference according to the dynamical phase difference Δ between the two probability amplitudes $|1 + e^{-i\Delta}|^2$. **c**. Only the qubit state in the upper path gains the geometric phase Φ_G induced by the sequential quantum measurements $\hat{A}$, $\hat{B}$ and $\hat{\Pi}^{\phi}$. The interference fringe is given by $|\alpha e^{i\Phi_G} + e^{-i\Delta}|^2$ and the geometric phase Φ_G can be extracted from the fringe shift. The coefficient α represents the relative amplitude difference between the two probability amplitudes and is due to quantum measurements on the qubit state in the upper path. BS, beam splitter.

One of the key features of our work is that we consider a generalized quantum measurement scenario in which the measurement can be weak: $\gamma \in [0, 1]$, where γ is the weak measurement strength. This has been achieved by introducing auxiliary qubits for registering the measurement outcomes[22]. The relevant quantum circuit is shown in Fig. 2a. Initially, the quantum state $|\psi\rangle_s$ is encoded in the system qubit and undergoes the sequential quantum measurement $\hat{\mathcal{M}}(\hat{A}, \hat{B})$ and is finally projected via the projector $\hat{\Pi}_s^{\phi}$. Specifically, an ancilla qubit is used to temporarily register the measurement outcome for the first observable $\hat{A}$. Conditioned on the ancilla state, the measurement interaction between system and meter qubits is realized for the observable $\hat{B}$. Then, erasing the information in the ancilla by projecting it on a certain basis ensures that only the meter qubit remains as the register for sequential observables $\hat{B}\hat{A}$ (refs. [35,36]). In other words, the system–meter interaction becomes $\hat{\mathcal{M}}(\hat{A}, \hat{B}) = \hat{B}\hat{A} \otimes \hat{\sigma}_x + (\hat{\mathbb{I}} - \hat{B}\hat{A}) \otimes \hat{\mathbb{I}}$. The meter qubit is flipped when $\hat{B}\hat{A}$ is applied, otherwise it is unchanged. In our scheme, the four possible measurement outcomes {00, 01, 10, 11} are essentially reduced to two outcomes. That is, the outcome '11' corresponds to the case in which the meter qubit is flipped, and the other three outcomes correspond to the case in which the meter qubit is unchanged. Since we are particularly interested in the case where $\hat{B}\hat{A}$ is applied, we consider only this case by projecting the meter qubit at the read-out process. Note that the measurement strength is determined according to the choice of projection basis for the meter state at the read-out. Using a single meter qubit makes not only the experimental set-up simpler, but also extracting the geometric phase easier. The geometric phase Φ_G induced by the quantum measurement for various measurement strengths is extracted by analysing the projected meter qubit state with the aid of the reference qubit. The reference qubit provides the phase reference to observe the geometric phase shift via quantum interference.

We have implemented the quantum circuit in Fig. 2a with photonic polarization qubits and path qubits (Fig. 2b). The system and meter qubits are encoded in the polarization mode of a single photon ($|H\rangle \equiv |0\rangle$, $|V\rangle \equiv |1\rangle$) and the ancilla and the reference qubits are encoded in the path mode of a single photon. Initially, the total quantum state for four qubits is prepared in $|\psi\rangle_s|0\rangle_a|+\rangle_m|0\rangle_r$, where $|\pm\rangle \equiv (|0\rangle \pm |1\rangle)/\sqrt{2}$. The subscripts {s, a, m, r} refer to system, ancilla, meter and reference qubits, respectively. After the single photon encoding the meter and reference qubits passes through the polarizing beam displacer (PBD), the total four-qubit quantum state is $|\psi\rangle_s|0\rangle_a \otimes (|1\rangle_m|0\rangle_r + |0\rangle_m|1\rangle_r)/\sqrt{2}$. A von Neumann type measurement interaction $\hat{\mathcal{M}}(\hat{A}, \hat{B}) = \hat{B}\hat{A} \otimes \hat{\sigma}_x + (\hat{\mathbb{I}} - \hat{B}\hat{A}) \otimes \hat{\mathbb{I}}$ is applied between the system qubit and the meter qubit with the aid of the ancilla qubit, conditionally if the state of the reference qubit is $|0\rangle_r$. Note that, for implementing $\hat{\mathcal{M}}(\hat{A}, \hat{B})$, we consider successive interactions acting on the system⊗ancilla⊗meter qubits: $\hat{U}_A = \hat{A} \otimes \hat{\sigma}_x \otimes \hat{\mathbb{I}} + (\hat{\mathbb{I}} - \hat{A}) \otimes \hat{\mathbb{I}} \otimes \hat{\mathbb{I}}$ and $\hat{U}_B = \hat{B} \otimes |1\rangle\langle 1| \otimes \hat{\sigma}_x + (\hat{\mathbb{I}} - \hat{B}) \otimes |1\rangle\langle 1| \otimes \hat{\mathbb{I}} + \hat{\mathbb{I}} \otimes |0\rangle\langle 0| \otimes \hat{\mathbb{I}}$. The ancilla qubit also needs to be projected onto $\hat{\Pi}_a^{+} = |+\rangle\langle +|$ so that $\hat{\Pi} = \hat{\mathbb{I}} \otimes \hat{\Pi}_a^{+} \otimes \hat{\mathbb{I}}$. Then, $\hat{\mathcal{M}}(\hat{A}, \hat{B}) = 2\,\mathrm{Tr}_a[\hat{\Pi}\hat{U}_B\hat{U}_A]$ (refs. [35,36]), where $\mathrm{Tr}_a[\cdot]$ is a partial trace over the ancilla qubit. See Methods for further details on the implementation of $\hat{\mathcal{M}}(\hat{A}, \hat{B})$. As the ancilla qubit has been traced out, the three-qubit state is calculated to be

$$\begin{aligned}&\{\hat{B}\hat{A}|\psi\rangle_s \otimes |0\rangle_m|0\rangle_r + (\hat{\mathbb{I}} - \hat{B}\hat{A})|\psi\rangle_s \otimes |1\rangle_m|0\rangle_r \\ &+ |\psi\rangle_s \otimes |0\rangle_m|1\rangle_r\} \;/\; \sqrt{2}\end{aligned} \tag{1}$$

Since the conditional interaction between the system and meter qubits defines the quantum measurement, the weak quantum measurement with the measurement strength $\gamma \in [0, 1]$ on the system qubit is defined by the rotation of the meter qubit $R(\theta_g)$, conditioned on the state of the reference qubit, and application of the projector $\hat{\Pi}_r^{1}$ to the reference qubit (Fig. 2a). In experiment, the conditional rotation of the meter qubit is accomplished with HWPs, as shown in Fig. 2b. If the reference qubit is in the state $|0\rangle_r$, the meter qubit is rotated with the HWP set with the angle θ_g such that $|0\rangle_m \to \cos 2\theta_g|0\rangle_m + \sin 2\theta_g|1\rangle_m$ and $|1\rangle_m \to \sin 2\theta_g|0\rangle_m - \cos 2\theta_g|1\rangle_m$. The case of $\theta_g = 0$ corresponds to the projection measurement, whereas the case of $\theta_g = \pi/8$ corresponds to the null measurement, as no measurement information is gained when projecting the meter qubit onto the computational basis[37]. The measurement strength γ is then related to the angle θ_g by the following relation, $\gamma(\theta_g) = 1 - 4/(3 + \cot 2\theta_g) \in [0, 1]$. Note that the measurement outcome for the sequential observable $\hat{B}\hat{A}$ is read-out by projecting the meter state onto the computational basis $\{|0\rangle_m, |1\rangle_m\}$ for the reference qubit $|0\rangle_r$. We consider the case when the meter state is projected onto $|0\rangle_m$ as it corresponds to the trajectory $\boldsymbol{\psi} \to \mathbf{a} \to \mathbf{b} \to \boldsymbol{\phi}$ in the limit of $\gamma \to 1$. The post-selection process is realized by considering a specific output port at the second PBD, as shown in Fig. 2b. See Supplementary Note 2 for further details. If the reference qubit is in the state $|1\rangle_r$, the HWP oriented at $\pi/4$ implements the operation $|0\rangle_m|1\rangle_r \to |1\rangle_m|1\rangle_r$ to pass the second PBD without photon loss. Finally, the projector $\hat{\Pi}_s^{\phi}$ is applied to the system qubit, thus making the system–meter qubit state as $\hat{\Pi}_s^{\phi}|\psi\rangle_s \otimes |\mathcal{M}\rangle_m$, where

$$|\mathcal{M}\rangle_m \propto \alpha e^{i\Phi_G}|0\rangle_m + \frac{\sqrt{5\gamma^2 + 2\gamma + 1}}{2\sqrt{2}}|1\rangle_m \tag{2}$$

and

$$\alpha e^{i\Phi_G} \equiv \frac{\left\langle \phi \middle| \frac{(1-\gamma)}{4}\hat{\mathbb{I}} + \gamma\hat{B}\hat{A} \middle| \psi \right\rangle}{\langle \phi | \psi \rangle} \tag{3}$$

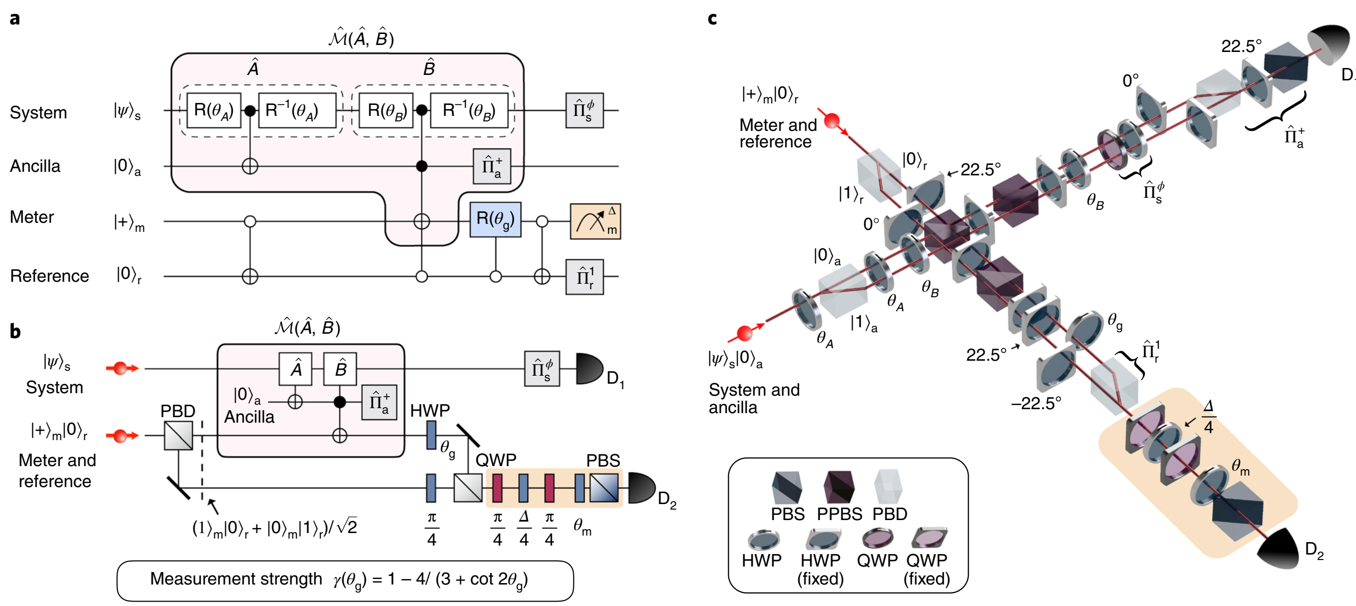

Fig. 2 | Schematic of the experiment. a. Quantum circuit for measuring the geometric phase due to quantum measurement back-action. Measurements $\hat{A}$ and $\hat{B}$, respectively, are set by $R(\theta_A)$ and $R(\theta_B)$. The sequential measurement $\hat{\mathcal{M}}(\hat{A}, \hat{B})$ between the system qubit and the meter qubit is mediated by the ancilla qubit and the measurement strength γ is set by $R(\theta_g)$. The system qubit is then projected by $\hat{\Pi}^{\phi}_s$ and the information on the ancilla and the reference qubits is erased by applying projections $\hat{\Pi}^{+}_a$ and $\hat{\Pi}^{1}_r$, respectively. The geometric phase Φ_G accumulated on the system qubit due to quantum measurement back-action is read out by measuring the meter qubit (see text for more details). **b**, Conceptual experimental set-up for the quantum circuit shown in **a**. The system and meter qubits are encoded in the polarization mode of a single photon and the ancilla and reference qubits are encoded in the path mode of a single photon. The meter and reference qubits are entangled by a CNOT operation: $(|1\rangle_m|0\rangle_r + |0\rangle_m|1\rangle_r)/\sqrt{2}$. The state $|1\rangle_m|0\rangle_r$ carries the information on the system qubit measured by observables $\hat{A}$ and $\hat{B}$ sequentially. To extract the geometric phase Φ_G on the system qubit, the meter qubit is scanned by rotating the HWP angle Δ with the measurement basis fixed at $\theta_m = 22.5°$. **c**, Schematic of the experimental set-up. The wave plates without denoted angles are fixed at 45°. The quantum measurement $\hat{\mathcal{M}}(\hat{A}, \hat{B})$ is implemented with two-photon quantum interference, thus allowing us to explore the quantum nature of the geometric phase (that is, the geometric phase due to quantum measurement back-action). PBS, polarizing beam splitter; PPBS, partially polarizing beam splitter; PBD, polarizing beam displacer; HWP, half-wave plate; QWP, quarter-wave plate.

Here, $\alpha \geq 0$ and Φ_G is the geometric phase due to quantum measurement.

In order to extract the geometric phase Φ_G, the final meter state in equation (3) is analysed with a set of a quarter-wave plate (QWP set at $\pi/4$), a half-wave plate (HWP set at $\Delta/4$), a quarter wave plate (QWP set at $\pi/4$), a half-wave plate (HWP set at θ_m), and a polarizing beam splitter (PBS), as shown in Fig. 2b. The coincidence count N between the detectors D_1 and D_2 then exhibits an interference fringe as a function of Δ. In particular, with the projection angle set at $\theta_m = \pi/8$, varying the HWP angle Δ in Fig. 2b has the same effect as scanning the path length difference in Fig. 1c. From equations (2) and (3), the coincidence count N is calculated to be

$$N \propto \left(\alpha^2 + \frac{5\gamma^2 + 2\gamma + 1}{8}\right) + \alpha\sqrt{\frac{5\gamma^2 + 2\gamma + 1}{2}}\cos(\Delta + \Phi_G + \theta_0) \quad (4)$$

where θ_0 is the initial phase factor. Hence, the geometric phase Φ_G due to quantum measurement corresponds to the phase shift from a reference interference fringe (that is, without the sequential measurement).

For the closed trajectory case, that is, $\boldsymbol{\phi} = \boldsymbol{\psi}$, we obtain

$$\Phi_G = \tan^{-1}\frac{\gamma\boldsymbol{\psi}\cdot(\mathbf{b}\times\mathbf{a})}{1 + \gamma(\mathbf{a}\cdot\boldsymbol{\psi} + \mathbf{a}\cdot\mathbf{b} + \mathbf{b}\cdot\boldsymbol{\psi})} \quad (5)$$

The above relation clearly demonstrates the fact that the geometric phase depends not only on the geometric vectors but also the measurement strength γ, which is related to the amount of quantum measurement back-action. Note that equation (5) reduces to the standard geometric phase derived from Pancharatnam's

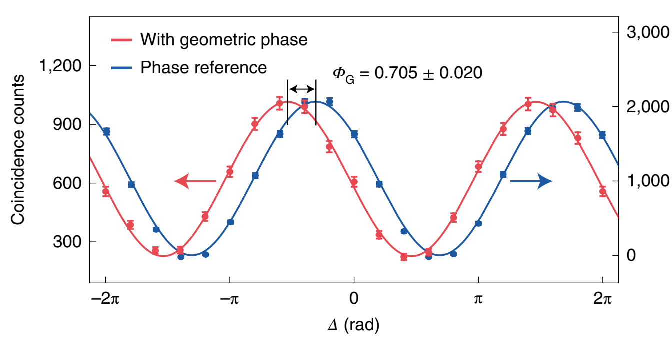

Fig. 3 | Extraction of the geometric phase. The measurement-induced quantum geometric phase Φ_G is extracted by comparing the polarization interferogram as a function of Δ in comparison to the reference interferogram. The experimental dataset for the measurement setting, $\boldsymbol{\psi} = \boldsymbol{\phi} = \{0, 1, 0\}$, $\mathbf{a} = \{0, 0, 1\}$ and $\mathbf{b} = -\{\sin(7\pi/13), 0, \cos(7\pi/13)\}$, is shown as red solid circles. For setting the reference phase, the condition for null measurement back-action is used by setting $\boldsymbol{\psi} = \mathbf{a} = \mathbf{b} = \boldsymbol{\phi} = \{0, 0, 1\}$ (see the blue solid circles). From the sinusoidal curve fitting (solid lines), the geometric phase is measured to be $\Phi_G = 0.705 \pm 0.020$ rad. The result is in a good agreement with the theoretical value of 0.725 rad. The error bar represents 1 s.d. due to Poissonian counting statistics.

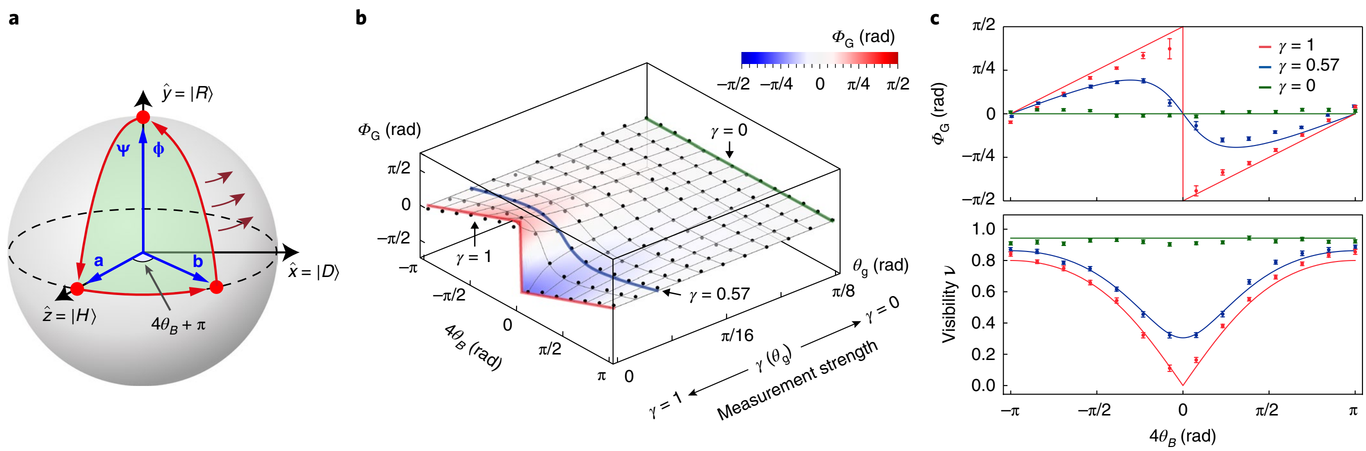

Fig. 4 | Emergence of the geometric phase from quantum measurement back-action. a, The quantum state trajectory based on the geodesic hypothesis due to sequential projective quantum measurements. The initial state $|\psi\rangle$, the final projection $\hat{\Pi}^{\phi}$, and the first measurement $\hat{A}$ are fixed, respectively, at $\boldsymbol{\psi} = \boldsymbol{\phi} = \{0, 1, 0\}$ and $\mathbf{a} = \{0, 0, 1\}$. The second measurement $\hat{B}$ is varied with $\mathbf{b} = -\{\sin 4\theta_B, 0, \cos 4\theta_B\}$ such that the geometric phase Φ_G is accumulated by increasing the angle θ_B. For weak measurements, it is in general not possible to define the corresponding vectors **a** and **b**. **b**, The measurement-induced geometric phase Φ_G as a function of the measurement direction θ_B and the measurement strength $\gamma(\theta_g)$. There is good agreement between the experimental data (black dots) and the theoretical result given by equation (6) (surface plot). **c**, The data show that the geometric phase is indeed due to quantum measurement back-action; that is, the stronger the measurements, the larger the accumulated geometric phase. When the measurement strength γ goes to zero, no geometric phase is observed because there are no changes to the quantum state due to the measurements (that is, no measurement back-action). Note that, at $\gamma = 1$, a sudden phase jump is observed. This singular behaviour can be understood by the geodesic hypothesis or by the fact that no phase can be defined as the visibility $\mathcal{V} = 0$ at this point. The error bars are obtained by performing 500 Monte Carlo simulation runs by taking into account the Poisson statistics in measured coincidence counts.

connection[2,3] when $\gamma \to 1$ (that is equation (5) is mathematically the same with the half-solid-angle subjected by the geodesic lines connecting the three vertices $\{\psi, a, b\}$ when $\gamma \to 1$). See Supplementary Note 1 for detailed derivation.

Experimental geometric phase

In experiment, the initial state and the final projection are set at $\boldsymbol{\psi} = \boldsymbol{\phi} = \{0, 1, 0\}$. The measurement $\hat{A}$ is fixed at $\mathbf{a} = \{0, 0, 1\}$ and the measurement $\hat{B}$ can be varied, $\mathbf{b} = -\{\sin 4\theta_B, 0, \cos 4\theta_B\}$. From equation (5), we then have

$$\Phi_G(\theta_B, \theta_g) = \tan^{-1}\left[\frac{\gamma(\theta_g)\sin 4\theta_B}{1-\gamma(\theta_g)\cos 4\theta_B}\right] \quad (6)$$

where $\gamma(\theta_g)$ is the measurement strength. Figure 3 shows a particular example of the interference fringe observed for $4\theta_B = 7\pi/13$ with $\gamma = 1$. The reference interference fringe is obtained with null measurement back-action by setting $\boldsymbol{\psi} = \mathbf{a} = \mathbf{b} = \boldsymbol{\phi}$ (that is by setting all observables to be commuting and the initial state to be their eigenstate). The interference fringe with geometric phase is shifted from the reference interference fringe by the amount $\Phi_G = 0.705 \pm 0.020$ rad. The experimentally extracted geometric phase from the phase shift measurement is in good agreement with the theoretically predicted value of 0.725 rad.

For the initial state and sequential projectors described above, the quantum state trajectory based on the geodesic hypothesis due to sequential projective quantum measurements (that is, $\gamma = 1$) is shown in Fig. 4a. Note that the $\hat{B}$ measurement direction is varied by choosing the angle θ_B. It is clear that, as the angle θ_B increases, the accumulated geometric phase Φ_G should get bigger as well. The experimental geometric phase due to quantum measurement as a function of the measurement strength $\gamma(\theta_g) \in [0, 1]$ and the measurement direction θ_B is shown in Fig. 4b. For the projection measurement ($\gamma = 1$), we observe the expected linear increase of the geometric phase with the increase of θ_B, but there is a sudden phase jump at $4\theta_B = 0$, more clearly shown in Fig. 4c. This singular behaviour is not observed in the geometric phase obtained via conventional unitary evolutions and it can be understood with the geodesic hypothesis of the state collapse due to quantum measurement. The geodesic hypothesis states that, when a qubit state is collapsed to an eigenstate due to a projective quantum measurement, the quantum state follows the geodesic line on the Bloch sphere during its collapse into the eigenstate[8,38]. The sudden phase jump observed in Fig. 4b,c for $\gamma = 1$ occurs when the vertices a and b are antipodal on the surface of the Bloch sphere so that no geodesic lines can be defined[39]. Therefore, our experimental results at $\gamma = 1$ can be regarded as a clear manifestation of the geodesic hypothesis[8,38]. Although the geodesic hypothesis is an essential prerequisite to reveal the measurement-induced geometric phase, it is a philosophical notion, as the state collapse is in fact discontinuous and instantaneous. It is also interesting that the continuous nonlinear stochastic model for the quantum measurement process also conforms to the collapse of a quantum state only when the geodesic trajectory is assumed[40]. The phase singularity[41] can also be seen by looking at the interference visibility. As depicted in Fig. 4c, when the phase jump occurs, the visibility becomes zero.

As the measurement becomes weaker ($\gamma < 1$), the measurement-induced geometric phase becomes smaller (Fig. 4b,c). Note also that the phase singularity no longer exists if $\gamma \neq 1$. Moreover, in experiment, we find that there is no measurement-induced geometric phase when $\gamma = 0$. This observation is consistent with the theoretical results in equations (5) and (6)

The expression for the geometric phase in equation (5) clearly indicates that the geometric phase is in fact due to quantum measurement back-action. The quantum measurement back-action refers to the fact that the quantum state of the measured system gets altered non-unitarily due to the measurement[22–24]. The numerator in the argument of $\tan^{-1}$ in equation (5), $\gamma\boldsymbol{\psi}\cdot(\mathbf{b}\times\mathbf{a})$, is in fact identical to $-2i\,\mathrm{Tr}(\gamma[\hat{B},\hat{A}]|\psi\rangle\langle\psi|)$, which quantifies the

Table 1 | Experimental results

$\boldsymbol{\phi}$	Experimental results
{0, 1, 0}	$\Phi_G = -0.519 \pm 0.016$, $\mathcal{V} = 0.850 \pm 0.011$
	$\langle \hat{B}\hat{A} \rangle_w^{\phi} = (0.484 \pm 0.012) - (0.276 \pm 0.010)i$
	$\langle \hat{B}\hat{A} \rangle_w^{\phi} = 0.433 - 0.250i$ [theory]
$\left\{\frac{1}{\sqrt{3}}, -\frac{1}{\sqrt{3}}, \frac{1}{\sqrt{3}}\right\}$	$\Phi_G = -0.014 \pm 0.013$, $\mathcal{V} = 0.945 \pm 0.010$
	$\langle \hat{B}\hat{A} \rangle_w^{\phi} = (0.712 \pm 0.023) - (0.010 \pm 0.009)i$
	$\langle \hat{B}\hat{A} \rangle_w^{\phi} = 0.683$ [theory]

The experimental geometric phase Φ_G, the interference visibility $\mathcal{V}$, and the extracted sequential weak value $\langle \hat{B}\hat{A} \rangle_w^{\phi}$ are shown for two different projector settings $\boldsymbol{\phi}$. The initial state is $\boldsymbol{\psi} = \{1/\sqrt{3}, 1/\sqrt{3}, 1/\sqrt{3}\}$. The observables $\hat{A}$ and $\hat{B}$ are projectors set to be $\mathbf{a} = \{0, 0, 1\}$ and $\mathbf{b} = \{1, 0, 0\}$, respectively. The results are in good agreement with the theoretical predictions. The errors are obtained by performing 500 Monte Carlo simulation runs by taking into account the Poisson statistics in measured coincidence counts.

incompatibility of two observables $\hat{A}$ and $\hat{B}$ as well as the measurement strength γ. As both $[\hat{B}, \hat{A}]$ and γ determine the degree of quantum measurement back-action, our result clearly identifies the quantum measurement back-action as the origin of the geometric phase—that is, the stronger the measurements, the larger the accumulated geometric phase[25].

Another interesting aspect of our work is that we able to experimentally demonstrate the connection between the geometric phase and the weak value, suggested theoretically in recent years[27–29]. An important and generally accepted notion on the weak value is that a weak measurement interaction (that is, $\gamma \ll 1$) is essential to extract the weak value. As such a weak measurement interaction would introduce almost no quantum measurement back-action, it is natural to ask why there would be a mathematical link between the geometric phase and the weak value[42,43].

To address the above question, we now consider the case $\boldsymbol{\phi} \neq \boldsymbol{\psi}$, that is, the quantum state trajectory is no longer cyclic. Then, in this condition, we immediately notice that equation (3) becomes the sequential weak value if $\gamma = 1$ (that is, $\alpha e^{i\Phi_G} \rightarrow \langle \hat{B}\hat{A} \rangle_w^{\phi} \equiv \langle \phi | \hat{B}\hat{A} | \psi \rangle / \langle \phi | \psi \rangle$). Therefore, the argument of the sequential weak value is identical to the measurement-induced geometric phase for the projection measurements. In other words, weak measurement interactions are no longer necessary for extracting the weak value[44–48]. Thus, the interference fringe measurement according to equation (4) for the open quantum trajectory allows us to extract the sequential weak value $\langle \hat{B}\hat{A} \rangle_w^{\phi}$ from strong measurement interactions ($\gamma = 1$) (see Methods for the details).

To demonstrate the sequential weak value measurement from projective measurements only, the initial state is set to be $\boldsymbol{\psi} = \{1/\sqrt{3}, 1/\sqrt{3}, 1/\sqrt{3}\}$. To consider the maximally incompatible observables $\hat{A}$ and $\hat{B}$, we choose $\mathbf{a} = \{0, 0, 1\}$ and $\mathbf{b} = \{1, 0, 0\}$. The experimental results, which show good agreement with the theoretical predictions, are summarized in Table 1. The sequential weak values for incompatible observables are known to be useful for direct characterization of quantum states and operations, such as density operators and quantum process matrices[35,49,50]. By using our approach, we have also carried out direct quantum state tomography exploiting sequential weak values via strong measurements. See Supplementary Note 1 for further discussions on the weak values and Supplementary Note 3 for the experimental direct quantum state tomography.

Conclusion

We have demonstrated theoretically and experimentally the geometric phase resulting from the quantum measurement back-action due to generalized quantum measurements by exploiting von Neumann measurement interactions with variable strengths. Our experiment has conclusively identified the quantum measurement back-action as the origin of the geometric phase in the measurement process, demonstrating the genuine quantum nature of the geometric phase. We hope our work triggers further studies to generalize our results to include higher dimensions and more observables. Finally, our investigation on the measurement-induced geometric phase has led us to connect the geometric phase to the weak value: in the limit of strong (projective) measurement, there is a direct connection between the geometric phase and the weak value. We believe that accessing the sequential weak value and the ability to perform direct quantum state/process characterization via only projection measurements will greatly improve the applicability of the weak value in experimental quantum information research.

Online content

Any methods, additional references, Nature Research reporting summaries, source data, extended data, supplementary information, acknowledgements, peer review information; details of author contributions and competing interests; and statements of data and code availability are available at https://doi.org/10.1038/s41567-019-0482-z.

Received: 5 November 2018; Accepted: 22 February 2019;
Published online: 15 April 2019

References

1. Berry, M. V. Quantum phase factors accompanying adiabatic changes. *Proc. R. Soc. Lond. A* **392**, 45–57 (1984).
2. Pancharatnam, S. Generalized theory of interference, and its applications. Part I. Coherent pencils. *Proc. Indian Acad. Sci. Sect. A* **44**, 247–262 (1956).
3. Berry, M. V. The adiabatic phase and Pancharatnam's phase for polarized light. *J. Mod. Opt.* **34**, 1401–1407 (1987).
4. Aharonov, Y. & Anandan, J. Phase change during a cyclic quantum evolution. *Phys. Rev. Lett.* **58**, 1593–1596 (1987).
5. Jordan, T. F. Berry phases for partial cycles. *Phys. Rev. A* **38**, 1590–1592 (1988).
6. Weinfurter, H. & Badurek, G. Measurement of Berry's phase for noncyclic evolution. *Phys. Rev. Lett.* **64**, 1318–1321 (1990).
7. Samuel, J. & Bhandari, R. General setting for Berry's phase. *Phys. Rev. Lett.* **60**, 2339–2342 (1988).
8. Cassinelli, G., De Vito, E., Lahti, P. & Levrero, A. Geometric phase and sequential measurements in quantum mechanics. *Phys. Rev. A* **49**, 3229–3233 (1994).
9. Sjöqvist, E. et al. Geometric phases for mixed states in interferometry. *Phys. Rev. Lett.* **85**, 2845–2848 (2000).
10. Kendric, B. K., Hazra, J. & Balakrishnan, N. The geometric phase controls ultracold chemistry. *Nat. Commun.* **6**, 7918 (2015).
11. Kenney, M. et al. Pancharatnam–Berry phase induced spin-selective transmission in herringbone dielectric metamaterials. *Adv. Mater.* **28**, 9567–9572 (2016).
12. Abdumalikov, A. A. Jr et al. Experimental realization of non-Abelian non-adiabatic geometric gates. *Nature* **496**, 482–485 (2013).
13. Sjöqvist, E. A new phase in quantum computation. *Physics* **1**, 35 (2008).
14. Loredo, J. C., Broome, M. A., Smith, D. H. & White, A. G. Observation of entanglement-dependent two-particle holonomic phase. *Phys. Rev. Lett.* **112**, 143603 (2014).
15. Laing, A., Lawson, T., López, E. M. & O'Brien, J. L. Observation of quantum interference as a function of Berry's phase in a complex Hadamard optical network. *Phys. Rev. Lett.* **108**, 260505 (2012).
16. Ericsson, M. et al. Measurement of geometric phase for mixed states using single photon interferometry. *Phys. Rev. Lett.* **94**, 050401 (2005).
17. Kwiat, P. G. & Chiao, R. Y. Observation of a nonclassical Berry's phase for the photon. *Phys. Rev. Lett.* **66**, 588–591 (1991).
18. Zhang, Y., Tan, Y.-W., Stormer, H. L. & Kim, P. Experimental observation of the quantum Hall effect and Berry's phase in graphene. *Nature* **438**, 201–204 (2005).
19. Leek, P. J. et al. Observation of Berry's phase in a solid-state qubit. *Science* **318**, 1889–1892 (2007).
20. Leonard, J. R. et al. Pancharatnam–Berry phase in condensate of indirect excitons. *Nat. Commun.* **9**, 2158 (2018).
21. Yale, C. G. et al. Optical manipulation of the Berry phase in a solid-state spin qubit. *Nat. Photon.* **10**, 184–189 (2016).
22. Hatridge, M. et al. Quantum back-action of an individual variable-strength measurement. *Science* **339**, 178–181 (2013).

23. Baek, S.-Y., Cheong, Y. W. & Kim, Y.-H. Minimum-disturbance measurement without postselection. *Phys. Rev. A* **77**, 060308(R) (2008).
24. Lim, H.-T. et al. Fundamental bounds in measurements for estimating quantum states. *Phys. Rev. Lett.* **113**, 020504 (2014).
25. Aharonov, Y., Kaufherr, T., Popescu, S. & Reznik, B. Quantum measurement backreaction and induced topological phases. *Phys. Rev. Lett.* **80**, 2023–2026 (1998).
26. Hong, C. K., Ou, Z. Y. & Mandel, L. Measurement of subpicosecond time intervals between two photons by interference. *Phys. Rev. Lett.* **59**, 2044–2046 (1987).
27. Sjöqvist, E. Geometric phase in weak measurement. *Phys. Lett. A* **359**, 187–189 (2006).
28. Tamate, S. et al. Geometrical aspects of weak measurements and quantum erasers. *New J. Phys.* **11**, 093025 (2009).
29. Cormann, M. & Caudano, Y. Geometric description of modular and weak values in discrete quantum systems using the Majorana representation. *J. Phys. A* **50**, 305302 (2017).
30. Aharonov, Y., Albert, D. Z. & Vaidman, L. How the result of a measurement of a component of the spin of a spin-1/2 particle can turn out to be 100. *Phys. Rev. Lett.* **60**, 1351–1354 (1988).
31. Cho, Y.-W., Lim, H.-T., Ra, Y.-S. & Kim, Y.-H. Weak value measurement with an incoherent measuring device. *New. J. Phys.* **12**, 023036 (2010).
32. Dressel, J. et al. Colloquium: understanding quantum weak values: basics and applications. *Rev. Mod. Phys.* **86**, 307–316 (2014).
33. Jordan, A. N. & Korotkov, A. N. Qubit feedback and control with kicked quantum nondemolition measurements: a quantum Bayesian analysis. *Phys. Rev. B* **74**, 085307 (2006).
34. Dressel, J., Agarwal, S. & Jordan, A. N. Contextual values of observables in quantum measurements. *Phys. Rev. Lett.* **104**, 240401 (2010).
35. Kim, Y. et al. Direct quantum process tomography via measuring sequential weak values of incompatible observables. *Nat. Commun.* **9**, 192 (2018).
36. Brodutch, A. & Cohen, E. Nonlocal measurements via quantum erasure. *Phys. Rev. Lett.* **116**, 070404 (2016).
37. Pryde, G. J. et al. Measurement of quantum weak values of photon polarization. *Phys. Rev. Lett.* **94**, 239904 (2005).
38. Facchi, P., Klein, A. G., Pascazio, S. & Schulman, L. S. Berry phase from a quantum Zeno effect. *Phys. Lett. A* **257**, 232–240 (1999).
39. Wong, H. M., Cheng, K. M. & Chu, M.-C. Quantum geometric phase between orthogonal states. *Phys. Rev. Lett.* **94**, 070406 (2005).
40. Patel, A. & Kumar, P. Weak measurements, quantum-state collapse, and the Born rule. *Phys. Rev. A* **96**, 022108 (2017).
41. Camacho, R. M. et al. Realization of an all-optical zero to π cross-phase modulation jump. *Phys. Rev. Lett.* **102**, 013902 (2009).
42. Curic, D. et al. Experimental investigation of measurement-induced disturbance and time symmetry in quantum physics. *Phys. Rev. A* **97**, 042128 (2018).
43. Bednorz, A., Franke, K. & Belzig, W. Noninvasiveness and time symmetry of weak measurements. *New J. Phys.* **15**, 023043 (2013).
44. Dressel, J. & Jordan, A. N. Weak values are universal in von Neumann measurements. *Phys. Rev. Lett.* **109**, 230402 (2012).
45. Vallone, G. & Dequal, D. Strong measurements give a better direct measurement of the quantum wave function. *Phys. Rev. Lett.* **116**, 040502 (2016).
46. Denkmayr, T. et al. Experimental demonstration of direct path state characterization by strongly measuring weak values in a matter-wave interferometer. *Phys. Rev. Lett.* **118**, 010402 (2017).
47. Cohen, E. & Pollak, E. Determination of weak values of quantum operators using only strong measurements. *Phys. Rev. A* **98**, 042112 (2018).
48. Calderaro, L. et al. Direct reconstruction of the quantum density matrix by strong measurements. *Phys. Rev. Lett.* **121**, 230501 (2018).
49. Thekkadath, G. S. et al. Direct measurement of the density matrix of a quantum system. *Phys. Rev. Lett.* **117**, 120401 (2016).
50. Mitchison, G., Jozsa, R. & Popescu, S. Sequential weak measurement. *Phys. Rev. A* **76**, 062105 (2007).

Acknowledgements

This work was supported by the KIST institutional programmes (project nos 2E29580 and 2E27800-18-P044), by the ICT R&D programme of MSIP/IITP (grant no. B0101-16-1355) and by the National Research Foundation of Korea (grant nos 2016R1A2A1A05005202 and 2016R1A4A1008978). Y.K. acknowledges support from the Global PhD Fellowship by the National Research Foundation of Korea (grant no. 2015H1A2A1033028).

Author contributions

Y.-W.C and Y.-H.K planned and supervised the research. Y.-W.C designed the experiment. Y.K., Y.-H.C., Y.-W.C. and Y.-S.K. performed the experiment. Y.-W.C., Y.K. and Y.-H.K. carried out the theoretical calculations, analysed data and discussed the results. Y.-S.K., Y.-H.C. S.-W.H., S.-Y.L. and S.M. contributed to the analysis and discussion of the results. Y.-W.C, Y.K. and Y.-H.K wrote the manuscript with input from all authors.

Competing interests

The authors declare no competing interests.

Additional information

Supplementary information is available for this paper at https://doi.org/10.1038/s41567-019-0482-z.

Reprints and permissions information is available at www.nature.com/reprints.

Correspondence and requests for materials should be addressed to Y.-W.C. or Y.-H.K.

Journal peer review information: *Nature Physics* thanks Andrew Jordan and the other anonymous reviewer(s) for their contribution to the peer review of this work.

Publisher's note: Springer Nature remains neutral with regard to jurisdictional claims in published maps and institutional affiliations.

Methods

Experimental details. The correlated photon pairs are generated via ultrafast pumped spontaneous parametric down-conversion at a 1 mm type-II beamlike beta barium borate (BBO) crystal. The photon pairs are then collected into single-mode fibres and delivered to the experimental set-up shown in Fig. 2c. Interference filters of 3 nm bandwidth centred at 780 nm are used for the high-visibility two-photon interference.

Implementation of $\hat{\mathcal{M}}(\hat{A},\hat{B})$. To implement the measurement interaction $\hat{\mathcal{M}}(\hat{A},\hat{B})$ between system and meter qubits, we introduce an ancilla qubit. The system–ancilla–meter joint quantum state is initially prepared in $|\psi\rangle_s|0\rangle_a|1\rangle_m$. In experiment, we exploit the path mode to encode the ancilla qubit as depicted in Fig. 2c. We consider successive interactions acting on the system⊗ancilla⊗meter qubits: $\hat{U}_A = \hat{A}\otimes\hat{\sigma}_x\otimes\hat{\mathbb{I}} + (\hat{\mathbb{I}}-\hat{A})\otimes\hat{\mathbb{I}}\otimes\hat{\mathbb{I}}$ and $\hat{U}_B = \hat{B}\otimes|1\rangle\langle 1|\otimes\hat{\sigma}_x + (\hat{\mathbb{I}}-\hat{B})\otimes|1\rangle\langle 1|\otimes\hat{\mathbb{I}} + \hat{\mathbb{I}}\otimes|0\rangle\langle 0|\otimes\hat{\mathbb{I}}$. The ancilla qubit also needs to be projected onto $\hat{\Pi}_a^+ = |+\rangle\langle +|$ so that $\hat{\Pi} = \hat{\mathbb{I}}\otimes\hat{\Pi}_a^+\otimes\hat{\mathbb{I}}$. Then, $\hat{\mathcal{M}}(\hat{A},\hat{B}) = 2\ \mathrm{Tr}_a[\hat{\Pi}\hat{U}_B\hat{U}_A]$ (refs.[35,36]), where $\mathrm{Tr}_a[\cdot]$ is a partial trace over the ancilla qubit. Note that $\hat{U}_A$ is a CNOT-type gate between the system and the ancilla qubits, which is realized with two HWPs (θ_A) and a PBD. $\hat{U}_B$ is a Toffoli-type gate operation, which is realized via a two-photon quantum-interference-based CNOT gate with PPBSs; $\hat{\Pi}$ is a simple projector for the ancilla qubit.

Extracting the weak value. The sequential weak value can be extracted from the interference fringe in equation (4) with $\gamma = 1$. The modulus and the argument of the weak value, respectively, are determined by the visibility $\mathcal{V} = 2\alpha/(\alpha^2+1)$ and the phase shift Φ_G (that is, $|\langle\hat{B}\hat{A}\rangle_w^\phi| = \alpha$ and $\arg\langle\hat{B}\hat{A}\rangle_w^\phi = \Phi_G$). Note that, from the visibility $\mathcal{V}$, there exist two mathematical solutions for α, the modulus of the weak value. One of the solutions is less than 1 and the other solution is larger than 1. Additional information is necessary to determine the correct value of α. Note that, from equation (4), if $N(\Delta, \theta_m = 0) < N(\Delta, \theta_m = \pi/4)$, then $\alpha < 1$, and if $N(\Delta, \theta_m = 0) > N(\Delta, \theta_m = \pi/4)$, then $\alpha > 1$. This relation is sufficient to determine the correct value of α. Note that $N(\Delta, \theta_m = 0)$ and $N(\Delta, \theta_m = \pi/4)$ are independent of Δ. Alternatively, one can use the following formulae to determine the real and imaginary values of the weak value:

$$\mathrm{Re}\langle\hat{B}\hat{A}\rangle_w^\phi = [N(0,\pi/8) - N(\pi/4,\pi/8)]/2N(\Delta,\pi/4)$$

$$\mathrm{Im}\langle\hat{B}\hat{A}\rangle_w^\phi = [N(3\pi/8,\pi/8) - N(\pi/8,\pi/8)]/2N(\Delta,\pi/4)$$

Data availability

The data that support the plots within this paper and other findings of this study are available from the corresponding authors upon reasonable request.